Ellipsometric study of percolation in electroless deposited silver films

Anna Jo de Vries, E. Stefan Kooij,[a] Herbert Wormeester, Agnes A. Mewe, and Bene Poelsema
Solid State Physics, MESA+ Institute for Nanotechnology, University of Twente, The Netherlands

(Received 27 October 2006; accepted 2 January 2007; published online 6 March 2007)

Using spectroscopic ellipsometry in the visible and near-infrared spectral range we investigate the optical properties of a growing silver film starting from predeposited gold nanoparticles. The effective pseudodielectric functions, obtained by direct inversion of the ellipsometry spectra, reveal a surface plasmon resonance for the nanoparticulate films. Upon prolonged electroless silver deposition, the resonance shifts to lower energies. The redshift is due the longer electron mean free path in larger silver structures and is analyzed by describing the optical response of the developing silver film in terms of a Lorentz line shape. The position of the oscillator, i.e., its resonance energy, is discussed in relation to the transition from isolated nanoparticles to an interconnected, eventually continuous metal film. This transition is also observed in the optical conductivity which exhibits an abrupt, stepwise increase at the same energy where the aforementioned resonance energy becomes zero. For longer deposition times, the optical spectra can be described in terms of a Drude-like free-electron metal. The development of the Drude–Lorentz parameters, i.e., the relaxation time and electron density, are compared to values for bulk silver; the latter were obtained from an optical measurement on a thick bulk silver sample. The saturation values for the relaxation time and thus the conductivity amount to approximately 40% of the bulk value, in agreement with direct current conductivity measurements on these films. © *2007 American Institute of Physics*.
[DOI: 10.1063/1.2654234]

I. INTRODUCTION

The growth of thin metal films is of relevance for a large range of application areas, including macroelectronics, microelectronics, and nanotechnology. Specific applications in the three aforementioned fields include thin film transitor displays, optical filters/sensors, and surface enhanced Raman spectroscopy sensors, respectively. Physical methods, as well as chemical routes for the growth of thin metal films have been pursued. In all cases, control over the growth process and the resulting film morphology is of paramount importance. For this reason, the formation of thin metal films has been receiving considerable attention in both fundamental and application oriented research.[1–13]

Recently, in developing an alternative metallization route via a nanocolloidal route, we explored the electroless growth of noble metals on predeposited gold nanoparticles.[14] The irreversibly deposited gold nanoparticles provide a well-defined seed structure for further metallization. Metal islands develop into larger superstructures to eventually yield macroscopically conducting films. The optical characteristics of the silver films grown using this soft, chemical approach, show very strong similarities to recently published work on physically deposited films via the plasma phase.[9–12]

In the work presented in this article, we investigate the optical properties of chemically deposited silver films on predeposited gold seed nanoparticles using spectroscopic ellipsometry. This technique provides a powerful means to monitor the developing silver films, both *ex situ* and *in situ*, in terms of deposited material, morphology and also electronic properties. We have chosen to study silver-on-gold growth since it provides a fast, reproducible, and technologically relevant system.

After a brief review of the sample preparation and silver growth methods, we describe the change of the direct current (dc) electrical conductivity with the increase of deposited silver. Subsequently, the shift of the surface plasmon resonance with prolonged silver growth, as exhibited in the optical spectra, is analyzed in terms of a Drude–Lorentz description. The results are compared to the dc conductivity and discussed in relation to previous work on similar systems,[1–13] in which the focus was on the determination of the percolation threshold in the transition from an island film, consisting of isolated metallic clusters, to a continuous, electrically conducting film. Additionally, we show that, in contrast to previously published work,[1,6,13] effective medium approximations in general fail to provide a proper description of the optical response of thin films near the percolation transition.

Finally, to enable a reliable comparison of the time-dependent Drude–Lorentz parameters, an ellipsometry measurement was performed on a bulk silver sample. From the optical response the bulk values for electron density and scattering rate were determined to be quite different from those derived on the basis of dc conductivity experiments. These discrepancies are discussed in relation to an absorption process in the midinfrared spectral range.

II. ELECTROLESS DEPOSITION OF SILVER FILMS

A. Synthesis of gold seed particles

Nanocolloidal gold suspensions were produced using the Frens method of citrate reduction.[15] Hydrogen tetrachloroaurate(III) hydrate (Aldrich) was dissolved in Milli-Q water

[a]Electronic mail: e.s.kooij@tnw.utwente.nl

(18.2 MΩ cm) to a 1 mM chloroaurate acid solution and trisodium citrate hydrate (Merck) to a 38.8 mM solution. While continuously stirring, 100 ml chloroaurate acid solution was heated to boiling under reflux conditions. Subsequently, 10 ml trisodium citrate solution was added. Typically within a few minutes gold nanoparticles are formed, exhibited by the final wine red color of the suspension. To allow completion of the reaction, the nanocolloidal suspension was kept at 100 °C for at least 15 min, after which it is left to cool down and stored at 4 °C. From transmission electron microscopy images, the diameter of the gold nanocrystals is estimated to be 12–13 nm.

B. Deposition of seed particles

Two types of silicon substrates were used having (i) a native oxide layer (approximately 2 nm thick) and (ii) a 215 nm thick oxide layer. The samples with a thick oxide layer were used in four-point probe conductivity measurements, where the oxide layer provides sufficient insulation of the silver layer to prevent shunting of the current through the substrate. To enable accurate quantitative analysis of ellipsometry spectra, samples with a native oxide layer are preferred. With the thick oxide layer samples, oscillations arising from interference of light reflected at both oxide interfaces complicate analysis of the results especially for low silver thicknesses. The silicon wafers were cut into 1 cm^2 samples and cleaned with Piranha solution (2:1 volume mixture of H_2SO_4 and H_2O_2) or ultrasonically in methanol. For amino-functionalization of the surface, the silicon substrates were immersed in a 10% solution of aminopropyltriethoxysilane (APTES, Merck) in methanol for 1 h. Subsequently, the samples were carefully rinsed with methanol, dried in a nitrogen flow, and finally immersed in water for 15 min to stabilize the siloxane bindings of the APTES molecule to the substrate surface and rinse off any access APTES.

The amino-functionalized substrates were immersed into the gold nanocolloidal suspension for approximately 12 h, ensuring that the surface coverage is saturated.[16] Subsequently, the samples were rinsed with water and dried in a nitrogen flow. A low gold particle coverage was obtained by tuning the ionic strength of the as-prepared suspension through 20-fold dilution with Milli-Q water.[17] From scanning electron microscopy images, such as those shown in Fig. 1, it was estimated that the surface coverage after immersion in the undiluted colloid amounts to 22%–23%, while for the 5% colloid the coverage was approximately 2%–6%. In the following, these are referred to as high and low coverage samples, respectively.

C. Seeded silver growth

The irreversibly adsorbed gold nanoparticles act as seeds for electroless deposition of silver. The silver deposition bath is based on the plating solution described by Tong *et al.*[18] The aqueous solution consists of 3.2 mM silver nitrate ($AgNO_3$, Merck), 100 mM hydrazine (hydrazine hydrate $NH_2NH_2 \cdot H_2O$, Acros Organics), 1.19 M ammonia (25% NH_3, Merck), and 0.27 acetic acid (CH_3COOH, Acros Organics).

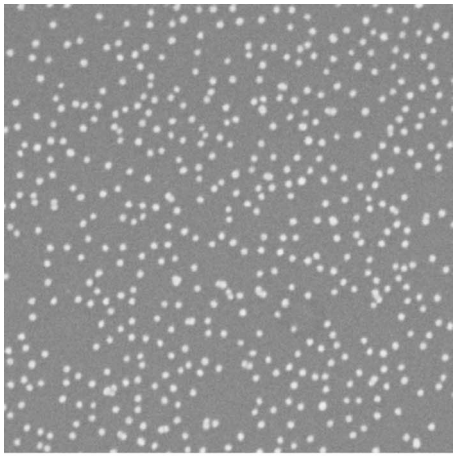

(a)

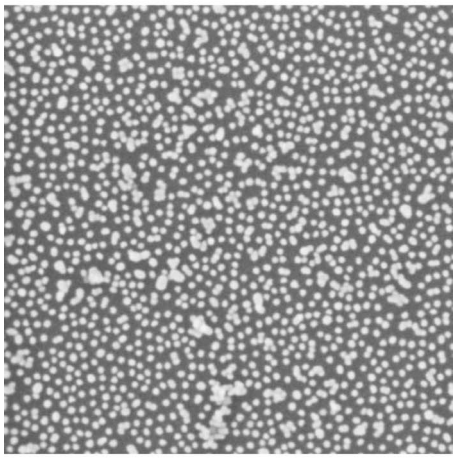

(b)

FIG. 1. Scanning electron microscopy images of samples with a low (a) and a high (b) coverage of gold nanoparticles after immersion into diluted and undiluted colloidal solution, respectively. The size of the images is 1 μm $\times$ 1 μm.

Silver deposition of a gold nanoparticle covered substrate is done by mixing all constituting chemicals. Silver nitrate is added last, immediately prior to immersion of the sample into the solution. To ensure reproducibility of the growth process, the sample was immersed during the deposition time while continuously stirring, then taken out and immediately rinsed using a flow of fresh demiwater and quickly dried in a flow of nitrogen. For the samples described in this work, the aforementioned procedure was repeated several times on the same sample to study the effects of increasing amounts of deposited silver on dc conductivity and ellipsometry spectra.

III. DC RESISTIVITY MEASUREMENTS

Conductivity measurements were performed with a Keithley model 2400 Sourcemeter, using a four-point probe on samples with a thick insulating oxide layer of 215 nm. From the resistance measurements, the conductivity of the layers is calculated using the thickness as determined from analysis of

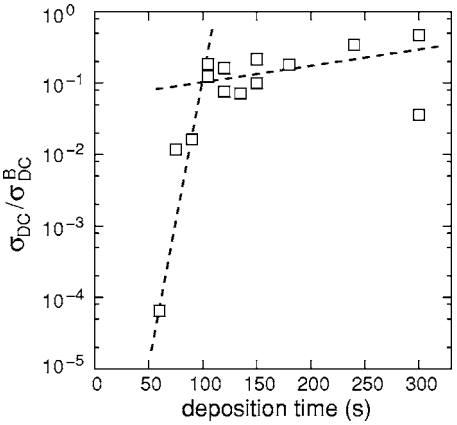

FIG. 2. Relative dc conductivity σ_{dc} of silver layers deposited on thick oxide samples with a high gold nanoparticle coverage, obtained by four-point probe measurements. σ^B_{dc} represents the bulk dc conductivity of silver which amounts to 63×10^6 S m^{-1}. The dashed lines are a guide to the eye.

ellipsometry spectra on the same samples. The experiments were performed on substrates with a high and a low gold coverage, obtained from immersion in a 100% and 5% gold suspension, as described in the previous section.

Four-point probe conductivity measurements on a series of samples are presented in Fig. 2. Results are shown for high gold nanoparticle coverages and silver deposited for increasing deposition times of up to 5 min. For deposition times shorter than approximately 60 s, the resistance of the layers is too large to accurately determine a conductivity value. Apparently, there is no current path available and the system is not yet in a percolated state. Between 1 and 2 min deposition time, the conductivity exhibits a strong increase. After approximately 2 min the conductivity still increases but markedly slower. The silver layer is past the percolation threshold and a path is available for dc electrical current. For prolonged silver deposition, the conductivity still increases slowly as a result of the additional amount of silver deposited, eventually filling the voids in the layer forming a more compact layer. The conductivity appears to saturate at about one-half of the bulk value $\sigma^B_{dc}=63\times10^6$ S m^{-1}. Considering the morphology of the film, and also the large density of grain boundaries, it is to be expected that the final conductivity is lower than that of bulk silver.

Conductivity measurements were also performed on samples with a low gold nanoparticle coverage (not shown in Fig. 2). In most cases, the resistance of the resulting silver layer was too high to be measured accurately by the four-point probe method. As an exception, for two samples, silver deposition during 5 min led to conductivity values less than 1% of the bulk conductivity.

IV. SPECTROSCOPIC ELLIPSOMETRY CHARACTERIZATION

A. Change of the pseudodielectric function

Ellipsometry measurements are performed *ex situ* using a Woollam variable angle spectroscopic ellipsometer (VASE), equipped with an adjustable compensator. An angle of incidence of 70° was used to measure the ellipsometric angles Ψ and Δ over the photon energy range 0.75–4.5 eV.

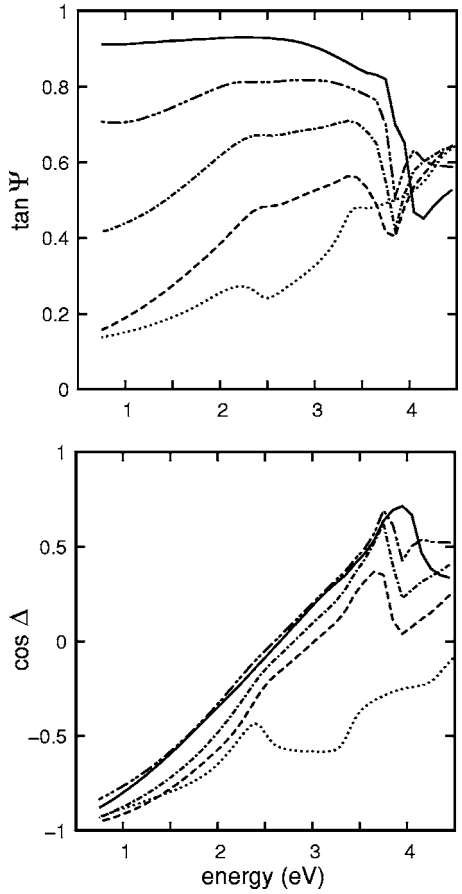

FIG. 3. Ellipsometry spectra of silver deposition for 0 s (dotted), 30 s (dashed), 1 min (dash-dotted), 2 min (dash-dot-dotted), and 5 min (solid) on a gold-seeded silicon/silicon oxide sample.

A series of ellipsometry spectra was measured for different silver deposition intervals. The silver was deposited in time steps of 15 s up to 2 min, followed by 30 s increments up to 5 min. After each immersion step, the samples were quickly and thoroughly rinsed with demiwater and then dried in a nitrogen flow. After each of the deposition steps an ellipsometry spectrum was measured. Experiments were performed both on samples with high and with low gold particle coverage. A selection of the measured spectra for a sample with silver deposition on a high gold particle coverage are shown in Fig. 3. Prior to silver deposition on the gold particulate layer, the plasmon resonance of the gold particles is visible as a characteristic feature near 2.4 eV in Fig. 3. Upon prolonged silver deposition, the gold plasmon resonance gradually diminishes to yield a spectrum comparable to that of bulk silver after 5 min. The optical response of bulk silver is characterized by the surface plasmon resonance near 3.7 eV. Similarly, the characteristic features of the substrate at higher energies also become less pronounced and gradually vanish.

A crude analysis of the optical properties of the growing silver films is performed on the basis of the ellipsometry spectra such as those in Fig. 3 by calculating the pseudodielectric functions considering the sample as a two-phase system, i.e., consisting of the sample and the ambient. The result is shown in Fig. 4. Before silver deposition, the dielectric function is dominated by the substrate features, which are

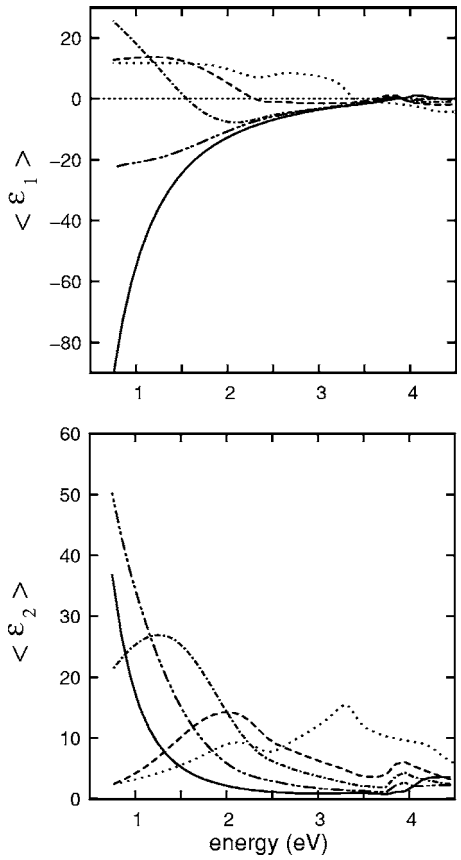

FIG. 4. Pseudodielectric functions after silver deposition for 0 s (dotted), 30 s (dashed), 1 min (dash-dotted), 2 min (dash-dot-dotted), and 5 min (solid), obtained by direct inversion of the spectra in Fig. 3, assuming a two-phase system.

most apparent at energies above 2.5 eV. The surface plasmon resonance of the gold nanoparticles is most clearly observed in the imaginary part of the pseudodielectric function by a maximum. Upon deposition of silver, the substrate response at high energies gradually vanishes, while the optical response for deposition times of 5 min and longer resemble that of an optically thick, i.e., bulk silver film. In agreement with this, the effective optical response reveals a distinct free electron contribution, exhibited by a strong increase of the imaginary component and a sharp decrease of the real part of the dielectric function for lower energies.

Oates and co-workers[9,10] describe and use a method to determine the percolation threshold of growing metal films, i.e., the moment at which the films become continuous to such an extent that macroscopic currents can be conducted. In their experiments on silver and titanium films on oxide substrates, the transition to an interconnected metal film is assumed to occur when the real part of the dielectric function becomes negative over the entire spectral range. Unfortunately, this implies that the extent of the spectral range considered in the optical experiments, has a significant influence on the actual result. In their experiments on silver island films[10] the spectral range of their ellipsometry spectra was limited to 1.5 eV on the low energy side. If we would apply this method to our data such as those in Fig. 4, and would only consider photon energies above 1.5 eV, percolation would already be concluded after 75 s of silver deposition. However, in the spectral range 0.8–1.5 eV these spectra exhibit an increase of the real part of the dielectric function even to positive values toward lower photon energies. On the basis of the present results, percolation is only after 2 min. Therefore, it appears that this method of determining the transition from a particulate to a continuous film introduces considerable uncertainty since the results depend very much on the accessible spectral range.

Furthermore, the aforementioned surface plasmon resonance feature, i.e., the peak in the imaginary component of the dielectric function in Fig. 4, shows a pronounced shift with prolonged silver deposition. This motivated us to perform a more specific analysis of the optical response in terms of a Lorentz oscillator.

B. Drude–Lorentz description of the growing metal film

Below the interband transitions at approximately 4 eV, the optical spectrum of silver is determined by the intraband transitions of the free electrons. For a free-electron like continuous metal film, the microscopic current is related to the applied external electric field by the so-called Drude function

$$\varepsilon_D = \varepsilon_\infty - \frac{E_p^2}{E^2 + i\hbar\frac{E}{\tau}}, \tag{1}$$

where $E_p = \hbar e\sqrt{N_e/m^*\varepsilon_0}$ is the bulk plasma energy, with N_e as the electron density, m^* as the effective electron mass, and τ as the characteristic electron relaxation time. The quantity ε_∞ takes into account interband transitions at energies exceeding the spectral range considered in the present experiments.

For a noncontinuous film, the movement of the free electrons is spatially limited therewith imposing a morphology dependent restoring force, which results in the so-called plasmon resonance. As an example, for a spherical silver particle (suspended in air), this leads to the well-known surface plasmon resonance at 3.5 eV. The optical response of this plasmon resonance can be described by a Lorentz line shape

$$\varepsilon_L(E) = \varepsilon_\infty + \frac{E_p^2}{E_0^2 - E^2 - i\hbar\frac{E}{\tau}}, \tag{2}$$

with E_p as defined earlier for the case of the Drude free electron contribution. The restricted volume, to which the free electrons are confined, leads to the plasmon resonance energy E_0, which is characteristic for the limited feature sizes. For nonspherical particles and also due to interaction of multiple particles, the plasmon resonance splits into low and high energy peaks, with the low energy feature having considerably larger intensity.[19,20] For a microscopically continuous film, i.e., beyond the percolation threshold, the plasmon energy E_0 will become zero, and transform the Lorentz line shape to the Drude expression given by Eq. (1).

The electron density N_e and the damping time τ have the same material property interpretation either in the case of a particulate or a percolated film. The resonance energy observed in these experiments is not directly related to the dielectric properties of silver as the growth occurs first on gold particles. However, the Lorentz shape will still occur for these all-metallic core-shell particles.

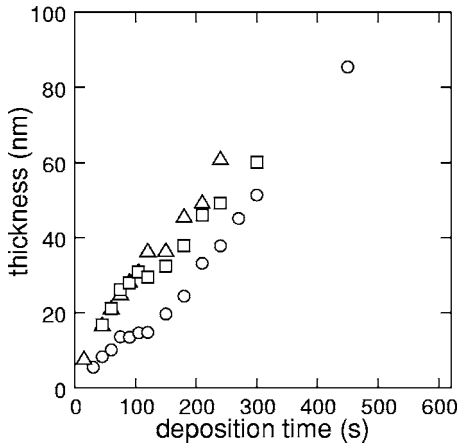

FIG. 5. Effective thickness of the layer as a function of silver deposition time, obtained from the fits. Results for high gold coverage (squares/triangles) and for low gold coverage (circles) are shown.

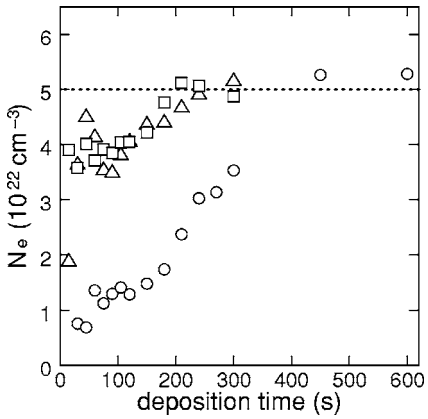

FIG. 6. Electron density N_e as a function of silver deposition time, for high gold coverage (squares/triangles) and low gold coverage (circles). The dashed line represents the electron density as determined for bulk silver.

In principle, nanometric cavities in a metallic film also give rise to plasmonic features, typically in the red to infrared range.[21] In the present work the optical response of nanoscale holes in the growing silver films is not observed. The absence of such plasmon resonances is ascribed to the poorly defined, irregular shape of the cavities.

C. Drude–Lorentz fit results

To obtain more quantitative information on the earlier description of the optical response of our developing silver films, we fitted the optical response assuming a three-phase model, i.e., by considering a substrate, the growing silver film and the ambient. To circumvent the large silicon-related features observed in Fig. 3 at high energies, we only consider the spectral range from 0.75 to 2.5 eV in our analysis. The sample, prior to silver deposition, including the gold nanoparticles, was described in the model by performing a point-to-point fit. A different approach in which the gold nanoparticles were modeled in terms of an effective medium approximation yielded very similar results. Significant deviations were only observed for short deposition times and in the energy range above 2.5 eV; this spectal range is not taken into account in our fits. In subsequent fits, the so-obtained effective optical response of the substrate was inserted into the model.

The growing silver film was modeled in terms of a single layer, of which the optical properties are described by one Lorentz line shape, as given by Eq. (2). Apart from ε_∞, there are four fit parameters to be considered. The Lorentz expression contains the effective electron concentration N_e, the relaxation time τ and the resonance energy E_0. Additionally, the layer thickness is incorporated as a fit parameter. To keep the number of fit parameters limited, we neglected any roughness in the silver film. This may introduce a considerable error primarily in the obtained thickness values.

The evolution of the effective film thickness of the silver layers with increasing deposition time, as obtained by the aforementioned procedure, is shown in Fig. 5 for both low and high gold coverage samples. From the first spectra the thickness could not be accurately determined. For a deposition time larger than 30 s a continuous increase in effective thickness can be observed. For the samples with high gold particle coverages, the initial increase in thickness is larger than for the low coverage. After two minutes of silver deposition the effective film thickness exhibits an approximately linear increase for both the high and low gold coverage with a similar growth rate of approximately 12 nm/min.

In Fig. 6 the time dependence of the charge carrier density N_e is shown. For the high gold coverage samples, the apparent electron density increases slightly, to reach the bulk silver value, indicated by the dashed line, after approximately 200 s. The bulk silver values will be discussed in the next section. For the substrate with a low initial gold coverage, the electron density saturates at the bulk silver value after more than 5 min. Also, the initial values of the electron density are considerably lower for the low seed particle coverage. We assume that the increase of the charge carrier density with deposition time arises from the particulate nature of the film. In our model we consider it to be a homogeneous, continuous film, while the rise in N_e reflects the increasing amount of metal in the layer.

The relaxation time τ, calculated from the fit using the Lorentz model, is shown in Fig. 7. In the case of the low gold particle coverage, the relaxation time exhibits a slow,

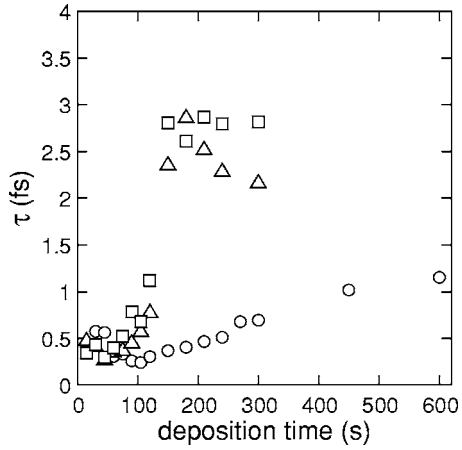

FIG. 7. Fit results of the relaxation time τ for silver deposition on high (squares/triangles) and on low gold coverage samples (circles).

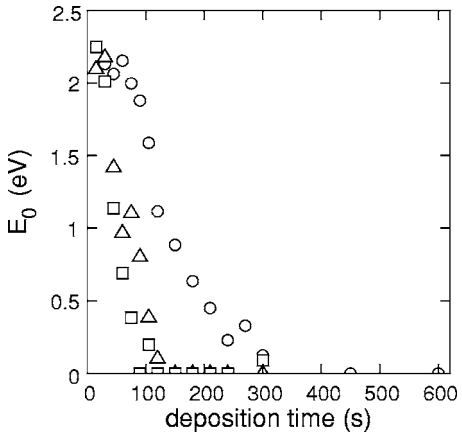

FIG. 8. Fit results for the resonance energy E_0, for silver deposition on samples with high (squares/triangles) and low gold coverage (circles).

gradual increase from 0.3 fs initially, to approximately 1 fs after 10 min of silver deposition. For the samples with a high gold seed particle coverage, the initial relaxation time, and its slow increase during the first minute, is similar to that of the sample with low gold coverage. This can be understood by considering that the relaxation time is primarily determined by the individual gold particles, on which the silver is deposited. After approximately 60 s, a more rapid increase of the relaxation time is observed, followed by an abrupt increase to approximately 3 fs after 130 s of silver deposition. We ascribe the distinct step of the relaxation time to a transition from isolated metal islands to a percolating metal film. A similar abrupt, stepwise increase of the relaxation time has also been reported by Nguyen and co-workers for thin aluminum films.[4] The saturation value of the relaxation time τ is markedly smaller than the bulk value. This will be discussed in more detail in the next section.

As mentioned in the previous section, the spectral features in Fig. 3 shift to lower energy with increasing silver growth time. This is also apparent from the resonance energy E_0 as a function of deposition time, as shown in Fig. 8. The initial value of E_0 for all samples is approximately 2.4 eV, which is close to the plasmon resonance energy of the gold nanoparticles prior to silver deposition. As expected, for both low and high gold seed coverage, the value of E_0 shifts to lower energy upon silver deposition. Owing to the lower limit of 0.8 eV of the spectral range in our experiments, the values of E_0 are only accurate above approximately 0.2 eV. Extrapolation of the values above 0.2 eV to zero indicates that, for the high gold coverage, E_0 vanishes after approximately 2 min while for the low seed density the transition from confined to free electrons is observed after 5 min silver deposition.

V. DISCUSSION

A. Thin film versus bulk silver

To enable a realistic comparison of the characteristics of our electroless grown silver films as determined from ellipsometry experiments in the visible and near-infrared range to those of bulk silver, we also performed an ellipsometry measurement on a clean bulk silver sample. A fit of the free electron contribution to the ellipsometry spectra in the range 0.75–2.5eV using the Drude expression given by Eq. (1) yields values for the charge carrier density and the relaxation time, $N_e=5.00\times10^{22}$ cm^{-3} and $\tau=6.7$ fs, respectively.

These values are markedly different from the bulk literature values $N_e=5.86\times10^{22}$ cm^{-3} and $\tau=40$ fs for bulk silver, established on the basis of dc electrical measurements. The considerable differences arise from the fact that our spectral range has a lower limit of 0.75 eV. Similar to the other noble metals gold and copper, the band structure of silver exhibits a feature in the mid-infrared, which gives rise to a slightly higher density of states in this energy range.[22,23] This leads to a contribution in the dielectric function of silver in the energy range 0.2–0.3 eV, which modifies the optical response in the visible and near-infrared range of the spectrum. Consequently, the free electron parameters obtained by fitting optical spectra yield results different from those obtained from dc electrical measurements. Similarly, the bulk resistivity $\rho_{ac}=10.6\ \mu\Omega$ cm as obtained from optical measurements is considerably larger than the dc electrical resistivity $\rho_{dc}=1.59\ \mu\Omega$ cm.

The charge carrier density and relaxation times for our electroless grown silver films, presented in the previous section, can now be compared to those of bulk silver, as determined optically. As indicated by the dashed line in Fig. 6, the electron densities exhibit a saturation for prolonged silver deposition at a value of $N_e=5.00\times10^{22}$ cm^{-3}, identical to that of bulk silver. The relaxation times for different silver deposition times, as shown in Fig. 7, can also be compared to the bulk data. After the formation of an interconnected but not fully continuous metal film, the values for our silver layers saturate at approximately 3 fs, less than half the optically derived bulk value of 6.7 fs. Apparently, the higher density of grain boundaries and other growth related defects gives rise to more electron scattering and thus shorter relaxation times as compared to bulk silver.

Considering that the imaginary part ε_2 of the dielectric function is proportional to the conductivity σ_{ac} at optical frequencies through

$$\varepsilon_2=\frac{\hbar\sigma_{ac}}{\varepsilon_0 E}, \tag{3}$$

where E is the photon energy, the "optical" conductivity can be derived by using Eq. (1) and setting the energy $E=0$ eV. We obtain

$$\sigma_{ac}=\frac{N_e\tau e^2}{m}, \tag{4}$$

where the electron density and the relaxation time are determined from the ellipsometry spectra. Similarly, the optical conductivity $\sigma_{ac}^{B}=9.4\times10^6$ S m^{-1} of bulk silver can be calculated from the fit parameters for a bulk silver sample. The thus obtained relative optical conductivities as a function of silver deposition time are shown in Fig. 9. As is to be expected, the deposition time dependence of the conductivity is very similar to that of the relaxation time. Especially for the high gold seed density this is obvious, since the variation of the electron density in Fig. 6 is less pronounced. Similar to

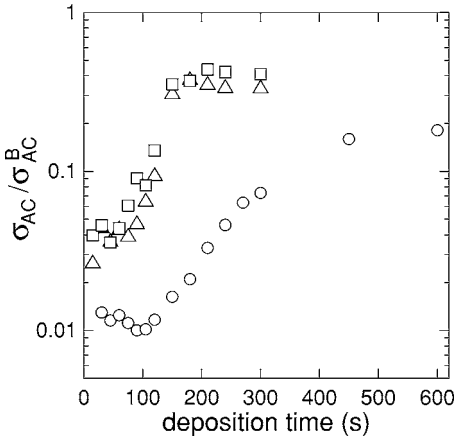

FIG. 9. Relative optical conductivity as a function of silver deposition time on samples with high (squares/triangles) and low (circles) gold coverage.

the dc conductivity results in Fig. 2, there is also a pronounced increase of the optical conductivity in Fig. 9. For longer deposition times both conductivities σ_{dc} and σ_{ac} exhibit a saturation. Despite the differences in the properties probed in both cases (for dc experiments, $E \ll 0.1$ eV), the values at which the relative conductivities saturate are comparable. For the dc conductivity, saturation is observed at approximately 0.3–0.5 times the bulk value, while the results in Fig. 9 show a maximum conductivity for prolonged silver deposition of approximately 0.4 times the bulk value.

For the samples with a low gold particle coverage, the optical conductivity increases gradually but does not exhibit the abrupt increase to higher values. Also, as mentioned in a previous section, the dc conductivity remains very low. Apparently, although the optical conductivity suggests that the silver islands grow (and cluster) during deposition, interconnection is not sufficient to allow the formation of a macroscopic current path, possibly due to the larger distance between the gold particles and thus between the silver islands.

B. Change in effective resonance energy

As described in the previous section, the growing silver layers studied in this work go through a transition from a particulate film, consisting of an isolated silver island on the gold seeds, to an interconnected, continuous structure after prolonged silver deposition. An important question often posed in relation to this and similar systems is how to determine the percolation threshold, or more precisely stated, the range in which the film goes through a transition from an electrically insulating film to a continuous, current conducting layer.

The conductivity, either optical or electrical, can provide an indication as to when percolation occurs. Surprisingly, however, comparison of the results in Figs. 2 and 9 indicates different silver deposition times at which the dc and optical conductivities, respectively, show a pronounced increase. For the samples with a high density of gold particles, the latter reaches saturation after approximately 150 s, while the dc conductivity values indicate that percolation is already established after approximately 100 s. Apparently, the fact that not the same properties are probed in dc and optical experiments yields different results.

Alternatively, the moment at which the resonance energy E_0 in Eq. (2) becomes zero, i.e., when the optical response can be described in terms of the Drude expression in Eq. (1), may be used as a probe for the aforementioned transition. For the high density of gold seed particles, the results in Fig. 8 indicate a deposition time of 130 s at which the films become Drude-like, consistent with the optical conductivity results. For the low seed particle densities, the resonance energy also shows a clear decrease to lower values and extrapolation to zero after 300 s seems reasonable. However, deposition time dependent conductivity measurements in Fig. 9 do not show distinct features characteristic of a percolation-like transition.

A more quantitative analysis of similar transitions as derived from optical spectra in a number of different systems has been attempted by several authors.[1–4,6,9–11,24] In most cases, the effective medium approximation established by Maxwell–Garnett is used as a basis. In principle, this is not very realistic, since the Maxwell–Garnett approach is only valid for low fill fractions of one material in a matrix of another material. Recently, it has been reported that the Maxwell–Garnett approach is also valid for higher fill fractions, if the positions of spherical inclusions in the matrix is uncorrelated;[13] this is not the case for our films.[17] Doremus has shown to obtain quite accurate results on the relation between the plasmon resonance of thin island films in relation to the coverage.[6] Despite the rather crude, in some cases uncertain assumptions in the model, the agreement between experiment and calculation is good, most likely due to the fact that only a very limited coverage range is considered.

By combining the Drude dielectric function in Eq. (1) (for an ideal free-electron metal with $\varepsilon_\infty = 1$) with the Maxwell–Garnett theory and considering an ambient dielectric function $\varepsilon_a = 1$, Yamaguchi[1] gives an expression for the effective dielectric function in relation to the fill fraction q in the layer

$$\varepsilon_{\text{eff}} = 1 + \frac{E_p^2 q}{\frac{1}{3}E_p^2(1-q) - E^2 + i\Gamma E}, \tag{5}$$

where E_p is the bulk plasma energy, corresponding to the electron concentration N_e. Doremus[6] uses a very similar approach. Comparison of this equation to the Lorentz line shape in Eq. (2) reveals the similarity between the two expressions. Moreover, there appears to be a direct relation between the strength [the enumerator in Eq. (5)] and the position [first term in the denominator in Eq. (5)] of the oscillator. The effective resonance energy is equal to $E_p\sqrt{(1-q)/3}$, which, in the limit of very low densities ($q = 0$) reduces to the surface plasmon resonance energy for spherical, metallic particles. Qualitatively, the behavior of the resonance energy with increasing fill fraction is similar to what we observe in Fig. 8. However, in this model, the resonance energy E_0 would only approach zero at a fill fraction $q = 1$, i.e., in case of a full layer. This is obviously not the case in our experiments.

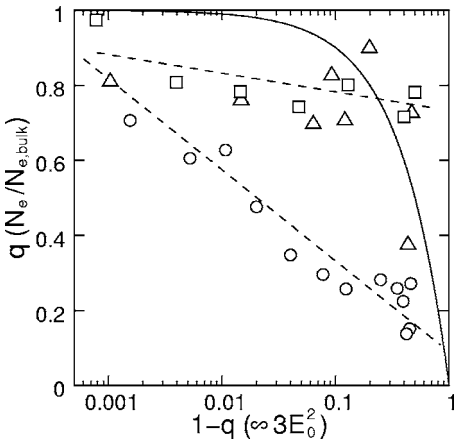

FIG. 10. Comparison of the electron density and resonance energies obtained from fitting our ellipsometry spectra to the Maxwell–Garnett model in Eq. (5) as presented by Yamaguchi (see Ref. 1). The symbols pertain to different series of experiments. The solid line represents the linear relationship (on a log scale) and the dashed lines are a guide to the eye.

We can compare our experimental results on the effective electron density in Fig. 6 and the resonance energy in Fig. 8 by plotting their relation as given by Eq. (5). When we plot the electron density, i.e., $N_e \propto E_p^2 q$, as a function of the square of the resonance energy E_0^2, a linear relation would be expected on the basis of Eq. (5), since $N_e=0$ for $q=0$ and $E_0=0$ for $q=1$. The comparison is shown in Fig. 10. Despite the qualitative agreement in that the electron concentration decreases for larger resonance energies, i.e., smaller fill fractions, the correspondence is far from linear (solid line in Fig. 10; note the logarithmic scale). Also, there is a distinct difference between the high and low seed density samples, which can also not be accounted for on the basis of Eq. (5). Despite the nonlinearity, there seems to be a relation between the two quantities (indicated by the dashed lines), which is markedly different for the high and low seed density samples.

In a more general treatment, the electromagnetic interaction between neighboring particles and/or islands, which is neglected in the Maxwell–Garnett approximation, has to be taken into account more explicitly. Also, in the derivation of Yamaguchi, the shape of the entities constituting the layer is assumed to be spherical, which is generally not the case. Contributions to the optical response of our silver layers, arising from interactions and shape, can be taken into account by considering that the parallel effective dielectric function $\varepsilon_{\text{eff}}^{\parallel}$ of a layer consisting of identical interacting dipolar particles, with area number density ρ are given by[25]

$$\frac{\varepsilon_{\text{eff}}^{\parallel}}{\varepsilon_a} = 1 + \phi\alpha_{\parallel}', \tag{6}$$

where $\phi=(\rho/d)(4/3)\pi a^3$ with d as the thickness of the layer and a as the particle radius. A similar expression also describes the perpendicular component of the dielectric function, but since our experiments are most sensitive to the low-energy parallel contribution, we will only focus on this component.

The dimensionless parallel polarizability of a generally ellipsoidal particle up to dipolar approximation is defined as

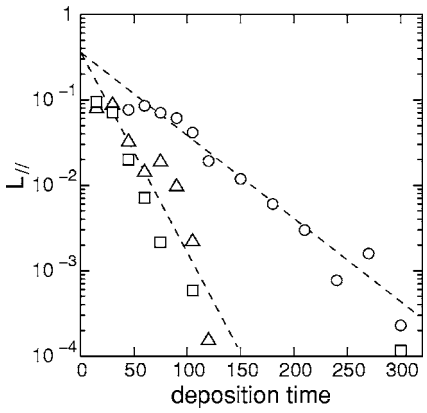

FIG. 11. Effective parallel depolarization factors as a function of the silver deposition time, for high (squares/triangles) and low (circles) seed particle density. The values have been calculated from the resonance energies E_0 in Fig. 8 using Eq. (8). The dashed lines are a guide to the eye.

$$\alpha_{\parallel}' = \frac{\varepsilon - \varepsilon_a}{\varepsilon_a + L_{\parallel}(\varepsilon - \varepsilon_a)}, \tag{7}$$

where ε and ε_a represent the dielectric functions of the constituting metal and the ambient, respectively. The depolarization factor $L_{\parallel}$ parallel to the substrate surface is related to the effective shape of the particles. For a sperical particle, the Claussius–Mossotti relation is obtained for $L_{\parallel}=1/3$. Inserting the Drude expression of Eq. (1) into Eq. (7), i.e., $\varepsilon=\varepsilon_D$, yields a Lorentz line shape, describing the localized nature of the electrons in our island films. The width Γ of the Lorentzian is equal to that of the Drude free electron gas, while the effective resonance energy for the interacting dipolar entities is given by

$$E_{0,\,\text{dip}}^2 = \frac{E_p^2}{\varepsilon_\infty + \left(\frac{1-L_{\parallel}}{L_{\parallel}}\right)\varepsilon_a}. \tag{8}$$

It is obvious that the effective resonance energy $E_{0,\,\text{dip}}$ is determined by the plasma energy, i.e., the charge carrier density, and also by ε_∞ and $L_{\parallel}$. The latter contains contributions from both the particle shape and electromagnetic interactions with neighboring particles.[20]

For a more quantitative analysis of the contribution of electromagnetic interactions to the optical response of our films, we can express the deposition time dependent shift of the resonance energy in Fig. 8 in terms of the effective depolarization factor $L_{\parallel}$ using Eq. (8). The result, using $\varepsilon_\infty=4$, $\varepsilon_a=1$, and $E_p=8.9$ eV, is shown in Fig. 11. It is obvious that the effective depolarization factor $L_{\parallel}$ decreases markedly with increasing silver deposition time. Linear extrapolation to short times of the data at longer deposition times (indicated by the dashed lines), indicates an initial value $L_{\parallel}=1/3$, which is expected for the spherical seed particles. The deviation from the dashed line at short silver deposition times may be due to inaccuracy of the fit results. Also, it can be ascribed to the nature of our film. We start with gold seeds onto which silver is deposited, implying a rather complicated system consisting of different materials. Initially, the optical

response is significantly influenced by the gold, which has a markedly different free electron contribution to the dielectric function ($\varepsilon_\infty = 10$ for gold).

An estimate of the contribution of interactions to the optical response of our electroless grown silver films can be obtained using our recent work, in which we have studied the collective optical properties of silver nanocrystal arrays.[20] In this work, the interactions between hexagonally ordered dipolar entities, with radius a in an array with lattice parameter r_0, were shown to give rise to an effective modification of the spherical response to oblate entities. Different polarizabilities parallel and perpendicular to the substrate have been expressed in terms of the corresponding depolarization factors. The effective depolarization factor $L_\parallel$ parallel to the substrate, on which the particles are assembled, was given by

$$L_\parallel = \frac{1}{3}\left[1 - \frac{S}{2}\left(\frac{a}{r_0}\right)^3\right], \tag{9}$$

where S represents the summation over all lattice sites. For a hexagonal lattice $S = 11.03$, while for a cubic lattice $S = 9.03$.[26,27] For the present work, we use the latter value, since we have previously found an approximately square-like distribution for irreversibly deposited gold nanoparticles.[17,28]

For a densely packed array of spherical particles, a maximum ratio $a/r_0 = 0.5$ is found, which yields an effective depolarization factor $L_\parallel = 0.15$ as determined using Eq. (9). The values for the depolarization factor shown in Fig. 11 are considerably lower than this value, indicating that not only electromagnetic interactions play a role. Apparently, also the shape of the growing silver islands is important, and even appears to be dominant in our case considering the markedly lower $L_\parallel$ values. In fact, this can be rationalized, by considering that the isolated seed particles grow isotropically into larger spherical entities. At a certain moment, adjacent islands will start to coalesce, resulting in effectively oblate silver islands. With increasing deposition time, more islands will grow together into even larger "pancake"-like clusters with an effectively increasing aspect ratio. For larger aspect ratios, the parallel depolarization factor decreases to very low values.[29] Correspondingly, the effective resonance energy in Eq. (8) will eventually decrease toward zero.

Finally, the dashed lines in Fig. 11 indicate that the time dependence of the effective depolarization factors is represented by an exponential decay $L_\parallel = 1/3\ \exp(-t/\tau_L)$, with τ_L some characteristic time scale. For the samples with a high seed density we find $\tau_L \approx 18$ s while for the low gold particle density $\tau_L \approx 40$ s is obtained. The relative difference between these values reflects the lower seed density, and thus a slower coagulation of the individual particles into larger oblate islands. An analysis of the absolute values for the characteristic times τ_L will require a more detailed modeling of the silver growth process, which lies outside the scope of this work.

VI. CONCLUSIONS

We have studied the optical properties of growing silver films using spectroscopic ellipsometry in the visible and near-infrared spectral range. The films are formed by electroless deposition of silver on irreversibly deposited gold nanoparticles. This implies that the metal layer develops from an island film, consisting of isolated metal clusters, into an interconnected superstructure to eventually grow into a continuous silver film.

The optical spectra, which show evidence of the transition from isolated metallic nanoclusters to an electrically conducting film, are analyzed in terms of a Lorentz oscillator. For short deposition times, the finite feature dimensions give rise to a localized plasmon resonance, exhibited by finite values for the resonance energy, i.e., the position of the Lorentz oscillator. Moreover, also the relaxation time as expressed by the inverse width of the oscillator has a very low value, in agreement with the localized nature of the conduction electrons within the metal nanoparticles.

Upon silver deposition on samples with a high seed particle density, the relaxation time eventually exhibits an abrupt increase to a value corresponding to approximately half the bulk value, indicating a transition to a macroscopic conducting state of the layer. The saturation values of the electron density and the relaxation time can be used to calculate the optical conductivity. In agreement with dc electrical conductivity experiments on similar films, the maximum value for the optical conductivity amounts to 40% of that of bulk silver. Apparently, a high density of defects, grain boundaries, and other impurities induces more scattering of the conduction electrons.

The resonance energy drops toward zero upon prolonged silver deposition. This is to be expected since, ultimately, a conducting silver film is formed, which can be described by Drude-like free electron behavior. The shift of the oscillator position as a function of silver deposition time has been analyzed in terms of the effective in-plane depolarization factor. Simple effective medium approaches based on the Maxwell–Garnett theory are shown not to provide an adequate description for the optical characteristics of metallic films near the percolation threshold.

Finally, the comparison of the optical alternating current (ac) and electrical dc conductivities leads to a surprising, relevant conclusion. The results indicate that the percolation behavior of growing silver (and also gold and copper), i.e., the transition from isolated metal islands to an interconnected, macroscopically conducting film as observed in optical experiments, is markedly different from that derived on the basis of dc resistivity experiments. Apparently, different properties relating to different energy ranges in the electronic band structure are probed in the various experiments.

ACKNOWLEDGMENT

This research is supported by the Stichting Technische Wetenschappen (STW), financially supported by the Nederlandse Organisatie voor Wetenschappelijk Onderzoek (NWO).

[1] S. Yamaguchi, J. Phys. Soc. Jpn. **15**, 1577 (1960).
[2] T. Yamaguchi, S. Yoshida, and A. Kinbara, Thin Solid Films **13**, 261 (1972).
[3] T. Yamaguchi, S. Yoshida, and A. Kinbara, Thin Solid Films **21**, 173 (1974).
[4] H. V. Nguyen, I. An, and R. W. Collins, Phys. Rev. B **47**, 3947 (1993).

[5]U. Kreibig and M. Vollmer, *Optical Properties of Metal Clusters* (Springer, New York, 1995).
[6]R. Doremus, Thin Solid Films **326**, 205 (1998a).
[7]A. Masten and P. Wissmann, Thin Solid Films **343–344**, 187 (1999).
[8]G. Fahsold, A. Priebe, N. Magg, and A. Pucci, Thin Solid Films **428**, 107 (2003).
[9]T. W. H. Oates, D. R. McKenzie, and M. M. M. Bilek, Phys. Rev. B **70**, 195406 (2004).
[10]T. W. H. Oates and A. Mücklich, Nanotechnology **16**, 2606 (2005).
[11]T. W. H. Oates, L. Ryves, M. M. M. Bilek, and D. R. McKenzie, Sens. Actuators B **109**, 146 (2005).
[12]T. W. H. Oates, Appl. Phys. Lett. **88**, 213115 (2006).
[13]P. Mallet, C. A. Guérin, and A. Sentenac, Phys. Rev. B **72**, 014205 (2005).
[14]A. A. Mewe, E. S. Kooij, and B. Poelsema, Langmuir **22**, 5584 (2006).
[15]G. Frens, Nature (London), Phys. Sci. **241**, 20 (1973).
[16]E. S. Kooij, E. A. M. Brouwer, H. Wormeester, and B. Poelsema, Colloids Surf., A **222**, 103 (2003).
[17]E. S. Kooij, E. A. M. Brouwer, H. Wormeester, and B. Poelsema, Langmuir **18**, 7677 (2002).
[18]H. Tong, L. Zhu, M. Li, and C. Wang, Electrochim. Acta **48**, 2473 (2003).
[19]E. S. Kooij and B. Poelsema, Phys. Chem. Chem. Phys. **8**, 3349 (2006).
[20]H. Wormeester, A. I. Henry, E. S. Kooij, B. Poelsema, and M. P. Pileni, J. Phys. Chem. **124**, 204713 (2006).
[21]J. Prikulis, P. Hanarp, L. Olofsson, D. Sutherland, and M. Kall, Nano Lett. **4**, 1003 (2004).
[22]M. A. Ordal, L. L. Long, R. J. Bell, S. E. Bell, R. R. Bell, R. W. Alexander, and C. A. Ward, Appl. Opt. **22**, 1099 (1983).
[23]H. Eckardt, L. Fritsche, and J. Noffke, J. Phys. F: Met. Phys. **14**, 97 (1984).
[24]R. Doremus, Thin Solid Films **326**, 205 (1998b).
[25]D. Bedeaux and J. Vlieger, *Optical Properties of Surfaces* (Imperial College Press, London, 2002).
[26]N. Pinna, M. Maillard, A. Courty, V. Russier, and M. P. Pileni, Phys. Rev. B **66**, 045415 (2002).
[27]R. G. Barrera, M. Delcastillomussot, G. Monsivais, P. Villasenor, and W. L. Mochan, Phys. Rev. B **43**, 13819 (1991).
[28]H. Wormeester, E. S. Kooij, and B. Poelsema, Phys. Rev. B **68**, 085406 (2003).
[29]H. C. van de Hulst, *Light Scattering by Small Particles* (Dover, New York, 1981).